with a matrix solution containing 10 mg/ml 3-hydroxypicolinic acid and 1 mg/ml diammonium citrate.

## Preparation of dumbbell-shaped RNA without nucleotide deletion

RNA without deleted nucleotide directed against human GAPDH was prepared as a single-stranded RNA, which then self-anneals into a structure containing 5′ and 3′ ends (**Figure 5**). The RNA 5′ end was phosphorylated by treating with T4 polynucleotide kinase (TaKaRa) in a reaction buffer containing 50 pmol RNA, enzyme 20 Units, 50 mM Tris-HCl, pH 8.0, 10 mM $MgCl_2$, 5 mM DTT and 1 mM ATP at 37°C for 2 h. After phenol/chloroform extraction and ethanol precipitation, the RNA 3′ and 5′ ends were ligated and the RNA converted to a circular type by treating overnight with T4 RNA ligase (TaKaRa) at 16°C in a reaction buffer containing RNA 2 ug, Enzyme 50 U, 50 mM Tris-HCl, pH7.5, 10 mM $MgCl_2$, 10 mM DTT, 1 mM ATP, 0.006% BSA. After phenol/chloroform extraction and ethanol precipitation, the formation of RNA was confirmed in 7 M urea-denatured 15% PAGE and by ESI-Q-TOF mass spectrometry. Dumbbell RNA was cut from the gel, extracted and purified using the small RNA Gel Extraction Kit (TaKaRa) following the manufacturer's instructions. The inhibitory activity of dumbbell RNA directed against human GAPDH was evaluated and compared with nkRNA in HCT 116 cell lines. The cells were treated with 1, 3, 10 nM of each RNA in the presence of lipofectamine 2000 and after 48 h mRNA was extracted from the cells and the amount of hGAPDH was quantified by real time PCR.

## Measurement of *Tm* values

*Tm* values of siRNA, nkRNA and PnkRNA in 50 mM phosphate buffer (PB), pH 7.5 or phosphate-buffered saline (PBS) were measured with UV-VIS spectrophotometers UV-1800 (Shimadzu Scientific Instruments., Japan), and analyzed with *Tm* Analysis software version 1,2,1,0 (Shimadzu Scientific Instruments, Japan).

## Quantitative real-time PCR

Total RNA was extracted from the cultured cells using RNeasy Mini Kit (Qiagen, Valencia, CA, USA), and cDNA was synthesized using SuperScript III (Invitrogen). To determine the mRNA knock-down level, Quantitative real-time PCR was carried out using the following primers (greiner Japan): human GAPDH, forward 5′-GGAGAAGGCTGGGGCTCATTTGC-3′ and reverse 5′-TGGCCAGGGGTGCTAAGCAGTTG-3′; human α-actin, forward 5′-GCCACGGCTGCTTCCAGCTCCTC-3′ and reverse 5′-AGGTCTTTGCGGATGTCCACGTCAC-3′, mouse TGF-β1, forward 5′-CCATTGCTGTCCCGTGCAGAGCTG-3′ and reverse 5′-ATGGTAGCCCTTGGGCTCGTGGATC-3′; mouse β-actin, forward 5′-GTCGTACCACAGGCATTGTGATGG-3′ and reverse 5′-GCAATGCCTGGGTACATGGTGG-3. Synthesized cDNAs were mixed with primers in Light Cycler Fast Start DNA Master SYBR Green I (Roche Diagnostics, Japan). Quantitative real-time PCR was performed using Light Cycler DX400 (Roche Diagnostics, Japan), and the reaction conditions were as follows: 95°C for 5 s, at 62°C for 15 s, and at 72°C for 15 s for 40 cycles (human GAPDH), or 95°C for 5 s, at 65°C for 15 s, and at 72°C for 15 s for 40 cycles (human β-actin, mouse TGF-β1, mouse β-actin). The data obtained from the assays were analyzed using Light Cycler Software version 4.1 (Roche Diagnostics, Japan). The mRNA knock-down levels were normalized with each β-actin transcript level.

## Animal model of acute lung injury (ALI)

Male C57/BL6 (8~9 week-old, weight, 22~24 g) mice purchased from Nihon SLC were used in the experiments. They were housed in the animal facility of Mie University, maintained on a constant 12-hour light/12-hour dark cycle in a temperature- and humidity-controlled room and were given food and water *ad libitum*. Under profound anesthesia (62.5 mg/kg intraperitoneal sodium pentobarbital) lung damage was induced by intratracheal (i.t.) instillation of LPS (5 mg/kg) dissolved in 50 μl of sterile saline (Nihon Kayaku) as previously described [24].

## Therapy of wild type mice with ALI using RNAi agents directed against TGF-β1

To assess the effect of nkRNA in acute lung injury, mice under anesthesia (intraperitoneal [i.p.] sodium pentobarbital) were treated with 100 μg of TGF-β1 nkRNA (nkRNA/LPS), scrambled nkRNA (control RNA/LPS), or vehicle (Vehicle/LPS) by intratracheal instillation one hour before LPS administration. Mice treated with i.p. injection of saline plus inhaled vehicle (vehicle/saline), TGF-β1 nkRNA (vehicle/TGF-β1 nkRNA) or scrambled nkRNA (vehicle/scrambled nkRNA) were used as control animals. The animals were sacrificed after 24 hours and BALF and lung tissue samples were taken for analysis.

For comparative analysis of the different RNAi agents, in a separate experiment, mice were treated with 100 μg of each siRNA (TGF-β1 siRNA/LPS), nkRNA (TGF-β1 nkRNA/LPS) and PnkRNA (TGF-β1 PnkRNA/LPS) directed against TGF-β1 or vehicle (vehicle/LPS) by i.t. instillation before LPS. Mice treated with i.p. injection of saline plus inhaled vehicle (vehicle/saline) were used as control animals. The animals were sacrificed after 24 hours and samples of BALF and lung tissue were taken for analysis.

## Therapy of human TGF-β1 TG mice with ALI using RNAi agents directed against TGF-β1

TGF-β1 bacterial artificial chromosome transgenic mice that express the human TGF-β1 gene specifically in the lungs under the control of the mouse SP-C promoter (hTGF-β1 TG) were used in these experiments. The hTGF-β1 TG mice spontaneously develop lung inflammation and fibrosis at 10 weeks of age as previously characterized [23]. To assess the therapeutic efficacy of RNAi agents in an ALI model closer to human conditions, hTGF-β1 TG mice were treated by i.t. instillation with 100 μg of each siRNA (hTGF-β1 siRNA/LPS), nkRNA (hTGF-β1 nkRNA/LPS) or PnkRNA (hTGF-β1 PnkRNA/LPS) directed against human TGF-β1 1 h before instillation of 100 μg LPS. Mice treated with vehicle (vehicle/LPS) and LPS were used as a positive control group and mice treated with 100 μg of control RNA (control RNA/LPS) and LPS were used as negative controls. Mice treated with i.p. injection of saline plus inhaled vehicle (vehicle/saline) were used as control animals. The animals were sacrificed after 24 h and BALF and lung tissue were taken for analysis.

## Therapy of wild type mice with pulmonary fibrosis using RNAi agents directed against TGF-β1

C57BL/6 wild type, female, 8 week-old (20~22 g) mice were used in the experiments. They were purchased from Nihon SLC (Hamamatsu, Japan) and maintained in Mie University's animal house. The Committee for Animal Investigation of Mie University approved the experimental protocol. Lung fibrosis was induced by 100 mg/kg bleomycin (BLM) dissolved in sterile saline administered to randomized mice by constant subcutaneous infusion using osmotic minipumps (model 2001; Alzet Corporation, Palo Alto,

CA) as previously described [23]; control mice received saline without BLM. RNAi agents against TGF-β1 (5 mg/kg) were administered i.t. on days 3, 7 and 14 after BLM. Controls were treated with i.t. scrambled RNAs (5 mg/kg) or vehicle. On the 21st day after BLM administration, all animals were sacrificed by i.p. overdose of pentobarbital to collect BALF, blood and organs. The degree of lung fibrosis was assessed by Ashcroft score and the tissue content of collagen and hydroxyproline was measured as previously described [23,25].

### BALF sampling

After euthanasia of the animals by i.p. anesthesia overdose, samples for biochemical and histological examinations were taken. Blood samples were collected by heart puncture and placed in tubes containing sodium citrate. Method for sampling of BALF in mice was previously described [23]. BALF total cell count was measured using a nucleocounter from ChemoMetec (Allerød, Denmark). The BALF was centrifuged and the supernatant was stored at −80°C until use for biochemical analysis. After cytospin separation of BALF cells, they were stained with May-Grunwald-Giemsa for differential cell counting (Merck, Darmstadt, Germany).

### Biochemical analysis

The level of protein was measured using commercial kits (BCA™ protein assay kit, Pierce, Rockford, IL) following the manufacturer's instructions. The levels of human and mouse TGF-β1 (R&D System, Minneapolis, MIN), interferon (IFN)-β and IFN-α (PBL Biomedical Laboratories, Piscataway, NJ) were measured using commercial EIA kits following the manufacturer's instructions.

### Lung histological findings

After euthanasia and thoracotomy, the pulmonary circulation was flushed with saline and then the lungs were excised. The lungs were perfused with 10% neutral buffered formalin, fixed in formalin and then embedded in paraffin. 5-μm thick sections of lung specimens were prepared and stained with Giemsa-eosin (Merck, Darmstadt, Germany) or hematoxylin-eosin and then examined under light microscopy (Olympus BX50 microscope, Tokyo, Japan).

### 5′-(Rapid Amplification of cDNA End) RACE assay

2 μg of total RNA from mouse lung tissue was used in the assays. First-strand cDNA synthesis was performed using the 5′-Full RACE Core Set (TAKARA) and the 5′ terminal-phosphorylated primer (5′-TGCAGGAGCGCACAA-3′). PCR was first performed using 1 μl of the first-strand cDNA synthesis reaction and primers (sense: 5′-AAGGTCCTTGCCCTCTACAACCAA-3′, antisense: 5′-TGTACTGTGTGTCCAGGCTCCAAA-3′). Reaction conditions were as follows: 98°C for 10 s, at 68°C for 30 s, and at 72°C for 30 s for 25 cycles. A nested PCR was then performed using 1 μl of the first-round reaction and primers (sense: 5′-TCCTTGCCCTCTACAACCAACACA-3′, antisense: 5′-TCCCAGACAGAAGTTGGCATGGTA-3′). Reaction conditions were as follows: 98°C for 10 s, at 68°C for 30 s, and at 72°C for 30 s for 35 cycles. Then, 10 μl of sample was analyzed on a 4% agarose gel.

## Supporting Information

**Figure S1 Representative HPLC chromatogram (black curves) and mass spectrum (red curves) of novel RNAi agents.** The purity and mass of each type of RNA are described in each corresponding box.
(PDF)

**Figure S2 Screening of mouse TGF-β1 nkRNA.** The inhibitory activity of varying concentrations of mouse TGF-β1 nkRNA and PnkRNA with deleted nucleotides (dn) at positions −2 (dn −2), −2 and −3 (dn −2, −3), 1 (dn 1) and 1 and 2 (dn 1, 2) was evaluated and compared; siRNA, nkRNA and PnkRNA caused a strong reduction in mTGF-β1 mRNA levels in Hepa 1–6 liver cells (A). nkRNA dn 1 and PnkRNA nd 1 against TGF-β1 also significantly decreased the target gene expression in lung epithelial cells (B). Statistical analysis by ANOVA. Data are expressed as the mean ± s.e.m. *$p<0.05$ vs cells treated with target nucleic acid agent.
(PDF)

**Figure S3 Digestion of nkRNA and PnkRNA by Dicer.** TGF-β1 nkRNA or PnkRNA, was incubated with Dicer as described under materials and methods for 0, 1, 3 and 6 h and degraded products were analyzed by mass spectrometry. Both nkRNA and PnkRNA were almost completely degraded by Dicer after 18 h (A). Mass spectrometry analysis (B, C) showed degradation products of 21~22 mers (S1, S2, A1, A2, A3) in length, which are the candidate siRNAs of both nkRNA and PnkRNA as described in **Table S4**.
(PDF)

**Figure S4 Comparative efficacy of siRNA, nkRNA and PnkRNA against mouse TGF-β1 in acute lung injury and confirmation of target degradation.** The concentration of TGF-β1 was measured by enzyme immunoassay in lung tissue homogenates. All siRNA, nkRNA and PnkRNA reduced the expression of target mRNA expression in the model compared to untreated mice (A). 5′-RACE analysis confirmed target degradation in the lungs after treatment with each agent (B). Statistical analysis by ANOVA. Data are expressed as the mean ± s.e.m.
(PDF)

**Table S1 Sequence of human GAPDH nkRNA with deleted nucleotide (dn) at different positions on the sense strand.**
(DOC)

**Table S2 Sequence of mouse TGF-β1 nkRNA and PnkRNA with deleted nucleotides at different positions and sequence of mouse TGF-β1 siRNA.**
(DOC)

**Table S3 Sequence candidates and mass of fragments released after Dicer digestion.**
(DOC)

**Table S4 Sequence of siRNA, nkRNA and PnkRNA directed against mouse TGF-β1 mRNA.**
(DOC)

**Table S5 Sequence of siRNA, nkRNA and PnkRNA directed against human TGF-β1.**
(DOC)

## Author Contributions

Conceived and designed the experiments: ECG HH T. Ohgi. Performed the experiments: TH PGB TK MT T. Matsumoto H. Shirohzu GNDG T. Mizutani MN DBR. Analyzed the data: ECG OT YE JM MK T. Ochiya T. Ohgi. Contributed reagents/materials/analysis tools: HH T. Ohgi TH H. Suzuki. Wrote the paper: ECG JM.

## References


1. Sledz CA, Williams BR (2005) RNA interference in biology and disease. Blood 106: 787–794.
2. Kim DH, Rossi JJ (2007) Strategies for silencing human disease using RNA interference. Nat Rev Genet 8: 173–184.
3. Bumcrot D, Manoharan M, Koteliansky V, Sah DW (2006) RNAi therapeutics: a potential new class of pharmaceutical drugs. Nat Chem Biol 2: 711–719.
4. Kedmi R, Peer D (2009) RNAi nanoparticles in the service of personalized medicine. Nanomedicine (Lond) 4: 853–855.
5. Pecot CV, Calin GA, Coleman RL, Lopez-Berestein G, Sood AK RNA interference in the clinic: challenges and future directions. Nat Rev Cancer 11: 59–67.
6. de Fougerolles AR (2008) Delivery vehicles for small interfering RNA in vivo. Hum Gene Ther 19: 125–132.
7. Chernolovskaya EL, Zenkova MA. Chemical modification of siRNA. Curr Opin Mol Ther 12: 158–167.
8. Lares MR, Rossi JJ, Ouellet DL. RNAi and small interfering RNAs in human disease therapeutic applications. Trends Biotechnol 28: 570–579.
9. Schlee M, Hornung V, Hartmann G (2006) siRNA and isRNA: two edges of one sword. Mol Ther 14: 463–470.
10. Judge AD, Sood V, Shaw JR, Fang D, McClintock K, et al. (2005) Sequence-dependent stimulation of the mammalian innate immune response by synthetic siRNA. Nat Biotechnol 23: 457–462.
11. Reynolds A, Anderson EM, Vermeulen A, Fedorov Y, Robinson K, et al. (2006) Induction of the interferon response by siRNA is cell type- and duplex length-dependent. RNA 12: 988–993.
12. Watts JK, Corey DR. Silencing disease genes in the laboratory and the clinic. J Pathol 226: 365–379.
13. Wilson MS, Wynn TA (2009) Pulmonary fibrosis: pathogenesis, etiology and regulation. Mucosal Immunol 2: 103–121.
14. Wynn TA (2008) Cellular and molecular mechanisms of fibrosis. J Pathol 214: 199–210.
15. Matthay MA, Zemans RL. The acute respiratory distress syndrome: pathogenesis and treatment. Annu Rev Pathol 6: 147–163.
16. Abe H, Abe N, Uda M, Tsuneda S, Ito Y (2009) Synthetic nanocircular RNA for controlling of gene expression. Nucleic Acids Symp Ser (Oxf): 65–66.
17. Abe N, Abe H, Ito Y (2007) Dumbbell-shaped nanocircular RNAs for RNA interference. J Am Chem Soc 129: 15108–15109.
18. Bartram U, Speer CP (2004) The role of transforming growth factor beta in lung development and disease. Chest 125: 754–765.
19. Lu Q, Harrington EO, Jackson H, Morin N, Shannon C, et al. (2006) Transforming growth factor-beta1-induced endothelial barrier dysfunction involves Smad2-dependent p38 activation and subsequent RhoA activation. J Appl Physiol 101: 375–384.
20. Madtes DK, Rubenfeld G, Klima LD, Milberg JA, Steinberg KP, et al. (1998) Elevated transforming growth factor-alpha levels in bronchoalveolar lavage fluid of patients with acute respiratory distress syndrome. Am J Respir Crit Care Med 158: 424–430.
21. Pittet JF, Griffiths MJ, Geiser T, Kaminski N, Dalton SL, et al. (2001) TGF-beta is a critical mediator of acute lung injury. J Clin Invest 107: 1537–1544.
22. Willis BC, Kim KJ, Li X, Liebler J, Crandall ED, et al. (2003) Modulation of ion conductance and active transport by TGF-beta 1 in alveolar epithelial cell monolayers. Am J Physiol Lung Cell Mol Physiol 285: L1192–1200.
23. D'Alessandro-Gabazza CN, Kobayashi T, Boveda D, Takagi T, Toda M, et al. (2012) Development and preclinical efficacy of novel transforming growth factor-beta1 siRNAs for pulmonary fibrosis. Am J Respir Cell Mol Biol 46: 397–406.
24. Takagi T, Taguchi O, Aoki S, Toda M, Yamaguchi A, et al. (2009) Direct effects of protein S in ameliorating acute lung injury. J Thromb Haemost 7: 2053–2063.
25. Ashcroft T, Simpson JM, Timbrell V (1988) Simple method of estimating severity of pulmonary fibrosis on a numerical scale. J Clin Pathol 41: 467–470.

# Inhibition of Stabilin-2 elevates circulating hyaluronic acid levels and prevents tumor metastasis

Yoshikazu Hirose[a,1], Eiko Saijou[a,1], Yasuyoshi Sugano[a,1], Fumitaka Takeshita[b], Satoshi Nishimura[c,d], Hidenori Nonaka[a], Yen-Rong Chen[a], Keisuke Sekine[a], Taketomo Kido[a], Takashi Nakamura[e], Shigeaki Kato[e], Toru Kanke[f], Koji Nakamura[f], Ryozo Nagai[c,d,g], Takahiro Ochiya[b], and Atsushi Miyajima[a,2]

[a]Laboratory of Cell Growth and Differentiation and [e]Laboratory of Nuclear Signaling, Institute of Molecular and Cellular Biosciences, University of Tokyo, Tokyo 113-0032, Japan; [b]Division of Molecular and Cellular Medicine, National Cancer Center Research Institute, Tokyo 104-0045, Japan; [c]Department of Cardiovascular Medicine, [d]Translational Systems Biology and Medicine Initiative, and [g]Global Center of Excellence Program, Comprehensive Center of Education and Research for Chemical Biology of the Diseases, University of Tokyo, Tokyo 113-8655, Japan; and [f]LivTech Inc., Kanagawa 216-0001, Japan

Edited by Joan Massagué, Memorial Sloan-Kettering Cancer Center, New York, NY, and approved February 3, 2012 (received for review October 31, 2011)

**Hyaluronic acid (HA) has been implicated in the proliferation and metastasis of tumor cells. However, most previous studies were conducted on extracellular matrix or pericellular HA, and the role of circulating HA in vivo has not been studied. HA is rapidly cleared from the bloodstream. The scavenger receptor Stabilin-2 (Stab2) is considered a major clearance receptor for HA. Here we report a dramatic elevation in circulating HA levels in Stab2-deficient mice without any overt phenotype. Surprisingly, the metastasis of B16F10 melanoma cells to the lungs was markedly suppressed in the Stab2-deficient mice, whereas cell proliferation was not affected. Furthermore, administration of an anti-Stab2 antibody in Stab2$^+$ mice elevated serum HA levels and prevented the metastasis of melanoma to the lung, and also suppressed spontaneous metastasis of mammary tumor and human breast tumor cells inoculated in the mammary gland. Administration of the antibody or high-dose HA in mice blocked the lodging of melanoma cells to the lungs. Furthermore, HA at high concentrations inhibited the rolling/tethering of B16 cells to lung endothelial cells. These results suggest that blocking Stab2 function prevents tumor metastasis by elevating circulating HA levels. Stab2 may be a potential target in antitumor therapy.**

cancer | hyaluronan | imaging | antibody therapy | sinusoid

Scavenger receptors mediate the endocytosis of metabolic waste products produced under normal and pathological conditions, as well as harmful foreign substances, such as bacterial debris absorbed in the gut. The liver functions as a major filter to eliminate such molecules from the circulation. Liver-specific capillaries known as sinusoids are vital to this function; for example, more than 90% of circulating hyaluronic acid (HA) is cleared by liver sinusoids (1). Sinusoidal walls consist of hepatic sinusoid endothelial cells (HSECs), stellate cells, and liver resident macrophages known as Kupffer cells. HSECs and Kupffer cells express various types of scavenger receptors to fulfill the filter functions. Among those scavenger receptors, Stabilin-1 (Stab1, also known as FEEL-1 and CLEVER-1) and Stabilin-2 (Stab2, also known as FEEL-2 and HARE) are structurally related, exhibiting 55% homology at the protein level, and expressed on HSECs (2).

Stab1 and Stab2 are large type I transmembrane glycoproteins containing four domains with EGF-like repeats, seven fasciclin-1 domains, and an X-link domain (3). Despite these two glycoproteins' structural similarity, the spectrum of their ligands differs significantly. Stab1 is expressed on lymphatic vessels and macrophages as well as HSEC and binds to acetylated low-density lipoprotein (ac-LDL), secreted protein acidic and rich in cysteine, placental lactogen, growth differentiation factor 15, and Gram-positive and Gram-negative bacteria, but not to HA (2, 4–8). It also mediates leukocyte trafficking (9). Stab2 is expressed on the sinusoid endothelium in the liver, spleen, and lymph nodes and has been used as a specific marker for HSECs (10). It binds to and mediates the endocytosis of HA, advanced glycation end products-modified protein, and heparin in addition to ac-LDL, growth differentiation factor 15, and bacteria (2, 4). Stab2 also recognizes membrane phosphatidylserine of apoptotic cells (11). Previous studies found that unlabeled chondroitin sulfate inhibited the uptake of $^{125}$-I-HA (12), and that ac-LDL binding to Stab2 was partially competed by heparin and dextran sulfate, but not competed by HA (13). These findings suggest that the HA binding site overlaps with the binding site of chondroitin sulfate but differs from the binding sites of ac-LDL, heparin, and dextran sulfate.

HA is a glycosaminoglycan of the extracellular matrix consisting of tandem repeats of D-glucuronic acid and *N*-acety-D-glucosamine. HA is abundant in the umbilical cord, articular joints, cartilage, and vitreous humor (14). It has been implicated in various physiological functions, including lubrication, water homeostasis, filtering effects, regulation of plasma protein distribution, angiogenesis, wound healing, and chondrogenesis (15). Signal transduction and functions of HA differ depending on molecular size; for example, high molecular weight HA suppresses angiogenesis, whereas HA fragments stimulate angiogenesis (16).

HA interacts with various cell surface receptors, including CD44, Lyve-1, TLRs, RHAMM, and Stab2 (17, 18). CD44, the most extensively characterized of these receptors, is expressed at varying levels in most immune cells and is involved in their rolling and extravasation via HA displayed on endothelial cells (ECs) (19). CD44 is also implicated in tumorigenesis and a marker for cancer stem cells (reviewed in ref. 20). Lyve-1 is structurally related to CD44 and is expressed in lymphatic vessels as well as in HSECs (21). TLR2 and TLR4 bind to HA or a complex of HA and HA-binding protein (18, 22); however, none of the mice deficient for CD44, Lyve-1, or TLRs have been shown to affect circulating HA levels in vivo. Although Stab1 and Stab2 are structurally related scavenger receptors with the HA-binding link domain, only Stab2 binds HA, and thus it has been considered the primary scanvenger receptor for HA (2, 3, 5).

HA, HA synthases (HAS), hyaluronidases, and HA receptors have been implicated in various tumors, including carcinomas, lymphomas, and melanocytic and neuronal tumors (23, 24). Overexpression and knockdown of HAS and hyaluronidases

Author contributions: Y.H., E.S., Y.S., H.N., and A.M. designed research; Y.H., E.S., Y.S., F.T., S.N., Y.-R.C., K.S., T. Kido, T.N., S.K., T. Kanke, K.N., R.N., and T.O. performed research; Y.H., E.S., Y.S., F.T., S.N., and A.M. analyzed data; and Y.H., E.S., and A.M. wrote the paper.

The authors declare no conflict of interest.

This article is a PNAS Direct Submission.

[1]Y.H., E.S., and Y.S. contributed equally to this work.

[2]To whom correspondence should be addressed. E-mail: miyajima@iam.u-tokyo.ac.jp.

This article contains supporting information online at www.pnas.org/lookup/suppl/doi:10.1073/pnas.1117560109/-/DCSupplemental.

have revealed that HA positively regulates proliferation, invasion, cell motility, multidrug resistance, and epithelial–mesenchymal transition in many tumor cell lines in vitro and in vivo (reviewed in ref. 23). Furthermore, an HAS inhibitor, 4-methylubelliferon, has been shown to decrease tumor proliferation and metastasis (25, 26).

Despite the importance of HA in tumorigenesis, assessing the role of circulating HA in tumor progression is difficult, because HA administered in the body is rapidly eliminated from the bloodstream (1). In this study, we generated Stab2 KO mice in which plasma HA levels were significantly elevated without any overt phenotype. Unexpectedly, tumor metastasis was markedly suppressed in these mice. We also found that administration of an anti-Stab2 antibody in WT mice elevated circulating HA levels and prevented tumor metastasis. Finally, we found that administration of a high dose of HA prevented the attachment of melanoma cells to the lungs in vivo and in vitro, and examined a possible link between circulating HA levels and tumor metastasis.

## Results

**Elevation of Circulating HA Levels in Stab2 KO Mice.** To address the physiological roles of Stab2 in vivo, we generated a Stab2 KO mouse line by replacing most of the first exon, including the ATG initiation codon and the first intron, with the LacZ and neomycin resistance genes (**Figs. S1 *A–C***). The lack of Stab2 expression in KO mice was confirmed by RT-PCR and immunostaining (**Figs. S1 *D* and *H*** and **S2*D***), Stab2-deficient mice were born according to the Mendelian ratio, grew normally, and showed no apparent abnormalities (**Fig. S1 *E* and *F***). Histological analyses revealed no significant changes (**Fig. S1*G***). Staining of liver sections with the anti-CD31 antibody, which binds HSECs as well as other types of ECs in the liver, demonstrated normal development of HSECs (**Fig. S1*H***). Furthermore, we found no significant differences in conventional diagnostic markers for functions of the pancreas, liver, and kidney (**Table S1**). These results indicate that Stab2 is dispensable for normal development and viability in mice.

Given that Stab2 is a known scavenger receptor that binds and eliminates from the circulation various substances, including HA, ac-LDL, and heparin (4, 27, 28), we assessed the circulating levels of these substances in Stab2 KO mice. Although serum levels of ac-LDL and heparin were unchanged in the Stab2 KO mice (**Table S1**), serum HA levels were dramatically increased, by as much as 59-fold over control values (Fig. 1*A*). Because HA's molecular size affects its function (16), we next analyzed the molecular size of serum HA by electrophoresis using Stains-All (which stains negatively charged molecules), and estimated it as ~40 kDa (**Fig. S1*J***). Given that >90% of the circulating HA is cleared by HSECs (1), and that Stab2 is specifically expressed in HSECs, we examined whether the high serum HA levels in Stab2 KO mice were due to impaired endocytosis. We prepared HSECs from WT and Stab2 KO mice and quantitatively evaluated their endocytotic activity based on the internalization of FITC-labeled HA and DiI-labeled ac-LDL (DiI-Ac-LDL) (Fig. 1*B* and *C* and **Fig. S1 *K* and *L***). Although there was no significant difference in the internalization of DiI-Ac-LDL between WT and Stab2 KO mice, the internalization of HA into Stab2-deficient HSECs was markedly decreased, to only ~8% of the WT level. We also examined the expression of other HA receptors (CD44 and Lyve-1) and HA synthases (HAS1, HAS2, and HAS3) that can potentially affect HA levels, but found no significant changes in the Stab2 KO mice (**Fig. S2 *A* and *B***). These results provide clear evidence that Stab2 is the major clearance receptor for HA in the body.

**Metastasis of Melanoma Cells Is Suppressed in Stab2 KO Mice.** The elevation in serum HA levels in Stab2 KO mice prompted us to examine whether the lack of Stab2 has any effects on tumorigenesis. B16 melanoma cells are known to form tumor nodules in the lung when injected i.v. We administered B16F10 cells i.v. in littermates of $Stab2^{+/+}$ and $Stab2^{-/-}$ mice. After 14 d, numerous black nodules had formed on the lung surfaces of the $Stab2^{+/+}$ mice, but surprisingly, nodular formation was markedly reduced in $Stab2^{-/-}$ mice (Fig. 2 *A* and *B*). In contrast, tumor formation resulting from the s.c. inoculation of melanoma cells did not differ significantly between the $Stab2^{+/+}$ and $Stab2^{-/-}$ mice (Fig. 2*C*). Moreover, our in vitro experiments showed that the proliferation of B16F10 cells was not affected by HA, and a cell cycle analysis of B16F10 cells recovered from lung tumors revealed no difference between the Stab2 KO and WT mice (**Fig. S3*A***). These results indicate that the metastasis, but not the proliferation, of melanoma cells was affected by the lack of Stab2.

To analyze the early stages of metastasis, we also conducted imaging in vivo, because the nodules of B16F10 cells at day 7 were too small to count. B16F10 cells were stably transfected with the firefly luciferase gene to generate B16F10-luc-G5 cells,

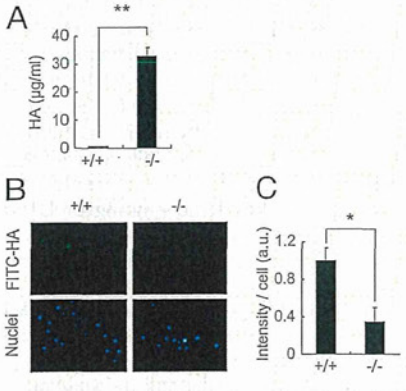


**Fig. 1.** Serum HA levels and internalization of HA in Stab2-deficient cells. (*A*) Serum HA levels in WT ($^{+/+}$) and homozygous ($^{-/-}$) littermates ($n = 3$; $^{**}P < 0.01$). (*B*) Internalization of FITC-HA in Percoll-purified HSECs from $Stab2^{+/+}$ and $Stab2^{-/-}$ littermates. (*Upper*) Fluorescence of FITC-HA incorporated into cells. (*Lower*) Hoechst 33342 staining. (*C*) Quantification of FITC fluorescence intensity ($n = 4$; $^{*}P < 0.05$).

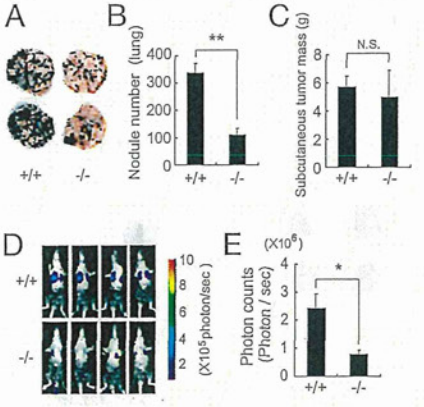


**Fig. 2.** Homing of B16F10 melanoma to the lungs in Stab2 KO mice. B16F10 cells ($5 \times 10^5$) were injected via the tail vein in $Stab2^{+/+}$ and $Stab2^{-/-}$ littermates. (*A*) Metastatic nodules formed on the lungs at day 14 after the injection. (*B*) Numbers of nodules formed on the lungs were counted manually ($^{+/+}$, $n = 9$; $^{-/-}$, $n = 6$; $^{**}P < 0.01$). (*C*) Size of tumors formed by s.c. inoculated melanoma cells at day 21 [$^{+/+}$, $n = 8$; $^{-/-}$, $n = 6$; $^{*}P > 0.05$ (not significant)]. (*D*) Metastasis of i.v. injected B16F10-luc-G5 cells measured by luminescence using IVIS in vivo imaging at day 7. (*E*) Quantification of photon counts in *C* ($^{+/+}$, $n = 6$; $^{-/-}$, $n = 5$; $^{*}P < 0.05$).

which were then injected i.v. into littermates of $Stab2^{+/+}$ and $Stab2^{-/-}$ mice. After 7 d, tumor metastasis was measured based on the luminescence of luciferase. Photon counts were significantly decreased in the $Stab2^{-/-}$ mice, indicating inhibition of metastasis at an early stage (Fig. 2 *D* and *E*).

**Administration of Anti-Stab2 Antibody Increases Serum HA Levels and Prevents Tumor Metastasis.** We next investigated whether Stab2 functions could be blocked by an anti-Stab2 antibody in vivo. We generated several mAbs against the extracellular domain of Stab2 by immunizing rats with BaF3 cells expressing Stab2 and one of them (#34-2, ref. 10) was found to inhibit HA binding to Stab2 as assessing by internalization of FITC-labeled HSECs in vitro (Fig. 3*A*). To test whether that anti-Stab2 mAb has any effect on the plasma HA level in vivo, we injected it i.p. into C57BL/6 mice every 3 d and monitored serum HA levels. Within 3 d of the first injection, serum HA levels were increased in all of the mice given the anti-Stab2 mAb, but not in the mice treated with rat IgG (Fig. 3*B*). We obtained the same results using SCID mice (Fig. 4 *A* and *J*). These findings clearly indicate that the anti-Stab2 mAb effectively increased plasma HA levels by inhibiting Stab2 function in vivo. To examine whether this mAb prevents tumor metastasis, we injected mice with either anti-Stab2 mAb or control rat IgG, followed 2 d later by i.v. injection of B16F10 cells. The anti-Stab2 mAb significantly suppressed metastasis (Fig. 3 *C* and *D*). Taken together, these results indicate that the anti-Stab2 mAb elevates circulating HA levels by blocking the clearance of HA in HSECs, and that serum HA levels are inversely correlated with tumor metastasis.

Because the anti-Stab2 mAb elevated plasma HA levels in immune deficient mice, we investigated its effect on spontaneous metastasis by multiple cancer cells in SCID mice. To do so, we transplanted MDA-MB-231-luc-D3H2LN cells (human mammary gland adenocarcinoma cells expressing luciferase) into the abdominal mammary glands of SCID mice. After 21 d, tumor metastasis in the upper body, including the brachial lymph nodes, was evaluated by luminescence analysis. The number of photons derived from metastasized cells in the upper body was significantly reduced in the mice treated with the anti-Stab2 mAb (Fig. 4*A–D*). We also transplanted 4T1-LucNeo-1H mouse mammary tumor cells expressing luciferase into the mammary fad pads of the mice. Starting at 2 d after tumor injection, each animal was given either anti-Stab2 mAb or rat IgG every 3 d. At 3 wk after the start of antibody treatment, metastatic luminescence signals and the numbers of histological lesions in the lung were reduced in the anti-Stab2 mAb-treated mice. Given the lack of significant difference in the size of primary tumors (Fig. 4 *E–L*), anti-Stab2 mAb can be considered to inhibit spontaneous metastasis.

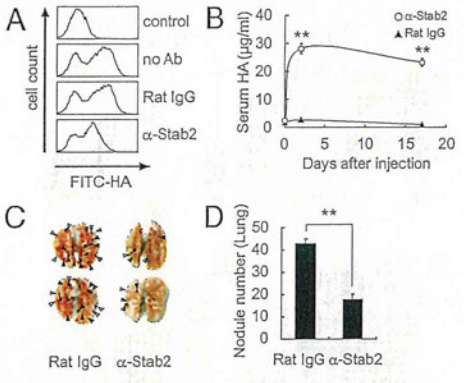


Fig. 3. Inhibition of HA clearance and metastasis by anti-Stab2 mAb. (*A*) HSECs were incubated with anti-Stab2 mAb or rat IgG, and the cell internalization of FITC-HA was analyzed by flow cytometry. (*B*) Anti-Stab2 mAb or rat IgG (3 mg/kg body weight) was administered i.p. to C57BL/6 mice on days 0, 3, and 17, and serum HA levels were measured ($n = 5$; $^{**}P < 0.01$). (*C*) At 2 d after the i.p. administration of anti-Stab2 mAb or control IgG, $5 \times 10^4$ B16F10 cells were injected i.v. via the tail vein. Anti-Stab2 mAb or control IgG was administered every 3 d. The lungs at 14 d are shown. Arrowheads indicate nodules of B16F10 cells. (*D*) The number of nodules formed on the lungs were counted manually ($n = 10$; $^{**}P < 0.01$). α-Stab2 denotes anti-Stab2 mAb.

**Examination of Possible Mechanisms for Inhibition of Metastasis.** To investigate the inhibitory mechanism of metastasis observed in the Stab2 KO and anti-Stab2 mAb-treated mice, we first analyzed whether HA affects tumor cells in vitro. We evaluated the effects of a 31-kDa HA (similar in size to HA in circulation; **Fig. S1*J***), on cell proliferation, apoptosis induced by hydrogen peroxide, migration, and invasion into the basal membrane. None of these assays demonstrated any significant effect of HA on tumor cells at various concentrations (**Fig. S3 *A–E***).

Because the proliferation as well as metastasis of tumors is under surveillance by the immune system, and HA has been implicated in the immune system, we examined the immune cells of Stab2 KO mice for any changes. We found no significant differences in fractions of regulatory T cells, NK cells, macrophages, and myeloid-derived suppressor cells in bone marrow, peripheral blood, and spleen in Stab2 KO mice compared with WT mice (**Fig. S4*A***). In addition, we found no alterations in serum levels of TNF-α, IFN-γ, IL-2, IL-4, IL-6 IL-10, and IL-17A (**Fig. S4*B***), or in the activation of macrophages in vivo and sensitivity to i.p. LPS (**Figs. S2*E*** and **S4*C***). These results showing no significant alterations in the immune system in Stab2 KO mice suggest that the immune system may not be directly involved in the inhibition of tumor metastasis.

**Attachment of Melanoma Cells to the Lungs Is Prevented by an Increase in Plasma HA.** Intravenously injected melanoma cells are thought to roll through the bloodstream and lodge in the lungs, where they proliferate. Our finding that the melanoma cells injected s.c. in Stab2 KO mice formed tumors as large as those seen in their WT littermates (Fig. 2*C*) suggests that the homing of i.v. injected tumor cells to the lungs might be altered in the mutant mice. To analyze the attachment of melanoma cells to the lung in vivo, we inoculated B16F10-luc-G5 cells i.v. After 6 h, mice were perfused with PBS via the portal vein to remove blood cells from the tissues, and luciferase activity in the lungs was evaluated. The luciferase activity in the lungs was significantly decreased in Stab2 KO mice and in mice treated with the anti-Stab2 mAb compared with WT mice and rat IgG-treated mice (Fig. 5 *A* and *B*). These results indicate that tumor metastasis was prevented at an early stage of penetration in the lungs.

Because plasma HA level has been suggested to be involved in the metastasis of melanoma cells, and HA binds to cell surface molecules such as CD44, we investigated whether HA mediates the attachment of tumor cells to tissues. We first tested the binding of melanoma cells to HA by plating B16F10 cells on an HA-coated plate, and found that the cells attached to the plate via HA (**Fig. S3*F***). Adding HA at the concentration found in Stab2 KO mouse sera inhibited the binding of B16F10 to the HA-coated plate. This finding suggests that the increased plasma HA in the mutant mice inhibits metastasis by preventing the attachment of melanoma cells to the lung via HA.

We also investigated whether HA prevents the attachment of B16F10 cells to the lung. Although i.v. injected HA is rapidly cleared from the bloodstream (1), we found that a very high dose of HA administered via the tail vain elevated the serum HA level for several hours (Fig. 5*C*). Thus, we injected HA at a dose of 20 mg/kg body weight every 8 h for 24 h to increase the plasma HA level, and then transplanted B16F10-luc-G5 cells. At 6 h after B16F10-luc-G5 cell transplantation, luciferase activity in the lungs was significantly reduced, whereas the serum

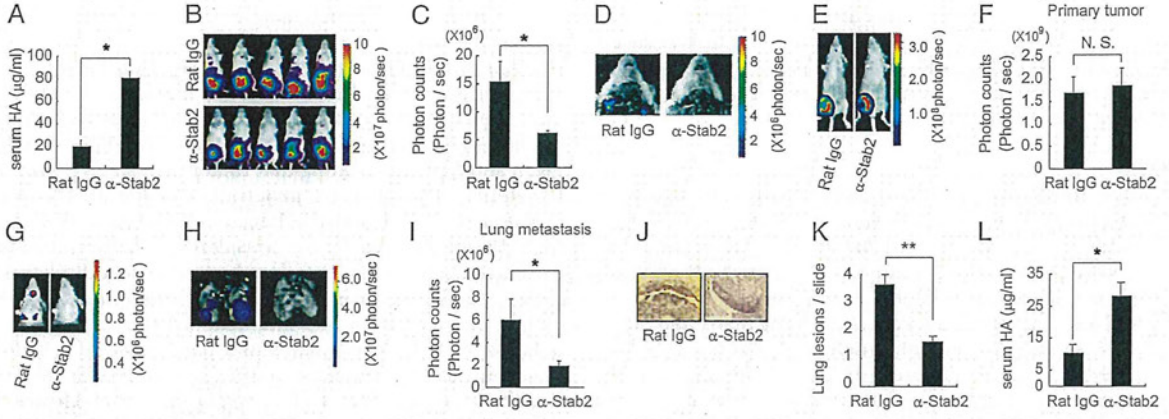


**Fig. 4.** Anti-Stab2 antibody prevents spontaneous metastasis of human and mouse mammary tumor cells in SCID mice. (*A*) SCID mice were i.p. injected with anti-Stab2 mAb or rat IgG (3 mg/kg), and serum HA levels were measured at 7 d after the injection ($n = 5$; $^*P < 0.05$). (*B*) MDA-MB-231-luc-D3H2LN cells were grafted in the mammary gland of SCID mice injected i.p. with anti-Stab2 mAb or control IgG (3 mg/kg). Luminescence was measured by IVIS at day 21. (*C*) Quantification of photon counts in the upper body at day 21 ($n = 5$; $^*P < 0.05$). (*D*) Luminescence of the opened thorax in *B*. (*E*) Mouse 4T1-LucNeo-1H mammary tumor cells were grafted into a mammary fat pad of the mice. At 2 d after tumor injection, each animal was given anti-Stab2 mAb or Rat IgG i.p. every 3 d, for a total of seven injections. Luminescence of primary tumors was measured by IVIS at day 21. (*G*) For the detection of signals from metastatic regions, the lower part of each animal was shielded with black paper before reimaging, to minimize bioliminescence from primary tumor. At the end of the experiment (day 21), ex vivo imaging was performed on collected lungs. Control group mice exhibited spontaneous lung metastasis. (*F*, *H*, and *I*) Quantification of bioluminescence emitted from primary tumors on mice and lung metastatic regions at the end of the experiment. Data represent mean ± SD ($n = 4$; $^*P < 0.05$ vs. other groups). (*J*) H&E-stained sections of spontaneous lung metastasis lesions at day 21. (*K*) Quantification of lung lesions in *J*. Data represent mean values ($n = 32$; $^{**}P < 0.01$ vs. other groups). (*L*) Serum HA levels measured at the end of the experiment ($n = 4$; $^*P < 0.05$). α-Stab2 denotes anti-Stab2 mAb.

HA level remained elevated in those mice pretreated with HA (Fig. 5 *D* and *E*).

Finally, to prove that increased HA level decreases the arrest of tumor cells in lung capillaries, we performed in vitro rolling/tethering assays using a VenaEC system. Pulmonary ECs from WT mice were cultured on VenaEC substrates and connected to a microfluidic device. Rolling/tethering between pulmonary cells and B16 melanoma cells under share stress was observed (Fig. 5*F*). At a low HA concentration (0.55 μg/mL, similar to Stab2$^{+/+}$ serum levels), B16 melanoma cells were tethered to pulmonary

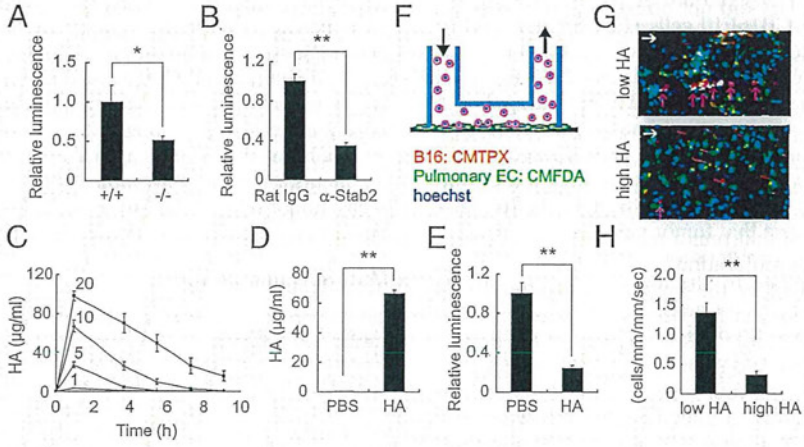


**Fig. 5.** HA inhibits attachment of B16F10 cells. (*A*) B16F10-luc-G5 cells ($1.5 \times 10^6$) were injected into the tail vein of Stab2$^{+/+}$ and Stab2$^{-/-}$ mice, and 6 h later, the mice were perfused with PBS via the portal vein to remove blood cells from tissues. The B16F10-luc-G5 cells remaining in the lungs were detected by luciferase analysis ($^{+/+}$, $n = 6$; $^{-/-}$, $n = 7$; $^*P < 0.05$). (*B*) At 2 d after the i.p. administration of anti-Stab2 or rat IgG, B16F10-luc-G5 cells ($1.5 \times 10^6$) were injected into the tail vein. At 6 h later, the injection cells remaining in the lungs were detected by luciferase analysis as in *A* (rat IgG, $n = 5$; $^{-/-}$, $n = 6$; $^{**}P < 0.01$). (*C*) HA at doses of 1, 5, 10, and 20 mg/kg was injected i.v., and serum HA levels were measured serially ($n = 4$). (*D*) HA at 20 mg/kg or an equal volume of PBS was injected i.v. every 8 h. At 24 h after the first HA injection, B16F10-luc-G5 cells ($1.5 \times 10^6$) were injected into the tail vein with 20 mg/kg of HA. After 6 h, serum samples were collected, and plasma HA levels were analyzed at the end of experiment ($n = 8$; $^{**}P < 0.01$). (*E*) Cells remaining in the lungs were detected based on luciferase activity at *D* as in *A* ($n = 8$; $^{**}P < 0.01$). (*F*) Schematic diagram of the VenaEC system (Cellix). (*G*) Rolling and/or tethering of B16 melanoma cells onto pulmonary ECs using the VenaEC system. Pulmonary ECs from 6-d-old WT (C57BL/6) mice were isolated, cultured, and stained with 5 μM CMFDA (green) and 10 μM Hoechst 33342 (blue). B16F10 cells were stained with 5 μM CMTPX (red) and 10 μM Hoechst (blue). The pulmonary cell chamber was connected to a microfluidic device, and perfusion for 5 min with VL medium containing stained B16F10 cells at 0.7 dynes/cm$^2$ was performed during confocal observation of cell kinetics. Representative images of B16 melanoma cells with low (0.55 μg/mL) and high (33 μg/mL) HA concentrations are shown (**Movies S1** and **S2**). White arrows denote flow directions, and red arrows indicate rolling and/or tethering B16F10 cells. (*H*) Quantification of rolling/tethering to the pulmonary ECs. The numbers of rolling/ tethering B16F10 cells were counted. Note that HA at high concentrations inhibited the rolling/tethering of melanoma cells onto pulmonary endothelium ($n = 20$ images from five experiments; $^*P < 0.05$). (Scale bar: 100 μm.) α-Stab2 denotes anti-Stab2 mAb.

cells. In contrast, at a high HA concentration (33 μg/mL, similar to Stab2$^{-/-}$ serum levels), tethering was significantly reduced (Fig. 5 *G* and *H* and Movies S1 and S2). These results indicate that a high level of HA in the circulation prevents the attachment of melanoma cells to the lung.

## Discussion

In this study, using Stab2 KO mice and an anti-Stab2 mAb, we provide several lines of evidence indicating that Stab2 is the major clearance receptor for circulating HA. This finding is consistent with the results of a previous in vitro study showing that Stab2, not its homolog Stab1, is the major clearance receptor for HA (5), as well as a recent study using Stab1 and Stab2 KO mice (2). In addition, KO mice deficient in either Lyve1 or Stab1 showed no change in serum HA levels (2, 29), further supporting this idea. Although Stab2 is known to bind other molecules, such as ac-LDL and heparin, serum levels of ac-LDL and heparin were not increased in the Stab2 KO mice, and the internalization of ac-LDL into Stab2-deficient HSECs was normal, indicating that those molecules are cleared by other scavenger receptors, such as Stab1. Therefore, we conclude that Stab2 is the bona fide clearance receptor for circulating HA in vivo.

An unexpected finding—and perhaps the most important result of this study—is the markedly reduced metastasis of melanoma cells in the Stab2 KO mice. Furthermore, i.p. administration of the blocking mAb for Stab2 also increased the serum concentration of HA and inhibited tumor metastasis in the Stab2$^{+/+}$ mice at levels comparable to those in Stab2 KO mice (Fig. 3). The KO mice were fertile, developed normally, and exhibited no hematological or histological changes except for the increased serum HA level (Fig. S1 and Table S1). Although Stab2 has multiple ligands, only HA levels were altered in the Stab2 KO mice, and the anti-Stab2 mAb caused phenotypes similar to those in the Stab2 KO mice. Thus, we focused on HA to investigate the mechanism preventing metastasis, and carried out various experiments in vitro and in vivo. Our in vitro experiments indicated that HA did not affect the proliferation, migration, and invasion of B16F10 cells (Fig. S3 *A–E*). Moreover, the weights of tumors formed by s.c. transplanted melanoma cells, as well as the cell cycle status of i.v. injected melanoma cells, were not changed in the Stab2 KO mice, indicating that the lack of Stab2 does not affect tumor proliferation in vivo (Fig. 2*C* and Fig. S3*B*). Likewise, mammary tumor cells formed primary tumors in abdominal fat pads, but tumor formation in the lymph nodes or lung was severely suppressed by anti-Stab2 mAb (Fig. 4). These results strongly suggest that tumor metastasis is prevented by a mechanism other than proliferation.

Tumorigenesis is controlled by the immune system, and the role of HA in the immune system has been studied extensively. Of note, HA binds to TLR2 and TLR4, which play important roles in innate immunity (18). We examined several parameters of the immune system, focusing first on macrophage functions, given that HA has been shown to alter immune responses via TLR4 that binds to LPS (18). However, macrophage activation and the severity of sepsis induced by i.p. injected LPS were not changed in Stab2 KO mice or in mice treated with the anti-Stab2 mAb (Figs. S2*E* and S4*C*). Furthermore, levels of inflammatory cytokines in serum and populations of various immune cells were not affected (Fig. S4 *A* and *B*). Therefore, inhibition of Stab2 function does not appear to directly affect the immune system. It is known that HA's functions depend on its molecular size, which varies from a few kDa to a few MDa (16). In the present study, HA molecules in Stab2 KO serum were ~40 kDa in size (Fig. S1*J*). possibly explaining some of the discrepancy between our results and those of previous studies.

Tumor cells circulate through the bloodstream and penetrate preferable tissues. Given that the s.c. proliferation of melanoma cells in Stab2 KO mice was not altered (Fig. 2*C*), we examined the initial step of attachment to the lungs. Melanoma cells expressing luciferase were injected via the tail vein, and cells trapped in the lungs were detected based on luciferase activity after perfusion with PBS to remove nonadherent cells. At 6 h after the i.v. injection, the number of melanoma cells trapped in the lungs was decreased in both the Stab2 KO mice and the mice given anti-Stab2, indicating that tumor metastasis is prevented at the initial stage of tissue penetration in the absence of Stab2 function (Fig. 5 *A* and *B*). Because those mice had extremely high plasma HA levels, we considered that the attachment of melanoma cells to the lungs is enhanced by HA displayed on the surface of blood vessels in normal lungs, and that a high level of HA in plasma blocks this interaction. In fact, melanoma cells adhered to HA-coated plates and pulmonary ECs, and HA at high concentrations, similar to those in serum of Stab2 KO mice, inhibited the attachment (Fig. 5, Fig. S3*F*, and Movies S1 and S2). Although i.v. injected HA is rapidly removed from the circulation, we found that the i.v. injection of a very high dose of HA was able to maintain the plasma HA concentration at a high level for at least 10 h (Fig. 5*C*). After the circulating HA level increased, B16F10 cells were injected to evaluate their attachment to the lungs. Metastasis of B16F10 cells to the lungs was markedly suppressed under these conditions (Fig. 3*D*). These results strongly suggest that inhibition of Stab2 function prevents tumor metastasis by elevating the plasma HA level.

Previous studies found that forced expression of HAS increased tumor cell proliferation and metastasis, whereas inhibition of HAS prevented proliferation and metastasis (23, 24, 30). These experiments suggested that HA promotes tumor proliferation and metastasis, whereas our results indicate that HA prevents metastasis. The critical difference between the previous studies and the present study is that we focused on the circulating HA, whereas most of the previous studies investigated extracellular matrix and pericellular HA. Therefore, it seems that the function of HA can differ depending on location.

In conclusion, our Stab2 KO mice were viable and exhibited no overt defects, but had dramatically increased plasma HA levels. This indicates that Stab2 is dispensable for normal development and homeostasis, and that an extremely high level of plasma HA has no deleterious effect. The increase in circulating HA levels was inversely correlated with metastasis and inhibited the attachment of melanoma cells to the lungs. Moreover, the administration of an anti-Stab2 mAb also increased the plasma HA level and blocked the metastasis of not only mouse melanoma cells, but also human breast tumor cells with no side effects. Thus, functional inhibition of Stab2 may be a potential strategy to suppress tumor metastasis.

## Materials and Methods

A Stab2 KO mouse line was generated by conventional methods, as described in *SI Materials and Methods*, and backcrossed with C57BL/6 for at least six generations. Anti-mouse Stab2 mAb (#34-2) was generated in our laboratory (10). Serum HA levels were measured with an HA assay kit (Seikagaku Biobusiness) in accordance with the manufacturer's instructions. The cell internalization of FITC-HA into HSECs was performed as described previously (10). For FACS analysis, HSECs were incubated with indicated antibodies and FITC-HA, and labeled cells were analyzed with a FACSCalibur flow cytometer (BD Biosciences). B16F10 cells [$5 \times 10^5$ (Fig. 2) or $5 \times 10^4$ (Fig. 3)] were injected into the tail vein. At 14 d after injection, the lung surface nodules were counted. For imaging in vivo, $5 \times 10^5$ B16F10-luc-G5 cells were injected i.v. At 7 d after the injection, metastasis was analyzed with luciferase luminescence as described previously (31). MDA-MB-231-luc-D3H2LN cells ($4 \times 10^6$) were injected into the mammary gland of SCID mice, and metastasis was analyzed using the IVIS imaging system (31, 32). 4T1-LucNeo-1H cells ($5 \times 10^4$) were injected into a mammary fad pad of SCID mice. Rolling and/or tethering of B16 melanoma cells onto cultured pulmonary ECs was analyzed under flow conditions at 0.7 dynes/cm$^2$ with the VenaEC System (Cellix) using confocal microscopy (Nikon A1R). Before the experiments, B16 melanoma cells were stained by CellTracker Red CMTPX (Molecular Probes) and Hoechst 33342 (Molecular Probes). Pulmonary ECs were also stained with CellTracker Green CMFDA (Molecular Probes) and Hoechst 33342. More detailed information is provided in *SI Materials and Methods*.

**ACKNOWLEDGMENTS.** We thank Dr. T. Akiyama for providing the B16F10 cells and Drs. H. Saya, T. Itoh, and M. Tanaka for valuable discussions and a critical reading of the manuscript. We also thank M. Tajima, C. Yoshinaga, and X. Yingda for their excellent technical help. This work was supported in part by research grants from the Ministry of Education, Culture, Sports, Science and Technology (MEXT) of Japan and the Ministry of Health, Labor and Welfare (MHLW) of Japan (to A.M.); the Centers of Research Excellence in Science and Technology program (A.M); the A-STEP program of the Japan Science and Technology Agency (Y.H.) and Takeda Science Foundation (to A.M.); the Funding Program for Next Generation World-Leading Researchers (to S.N.); the Japan Society for the Promotion of Science through its Funding Program for World-Leading Innovative Research and Development on Science and Technology (FIRST Program) (R.N.); Research Fellowships from a Grant-in-Aid 22113008 for Scientific Research on Innovative Areas of Fluorescence Live Imaging from The Ministry of Education, Culture, Sports, Science, and Technology of Japan (to S.N.); Grants-in-Aid for Scientific Research (to R.N.), grants for Translational Systems Biology and Medicine Initiative (to S.N. and R.N.), and the global Centers of Excellence program from the MEXT of Japan (R.N.); Banyu Life Science Foundation International (S.N.); and a research grant from the National Institute of Biomedical Innovation (to R.N.).

1. Fraser JR, Alcorn D, Laurent TC, Robinson AD, Ryan GB (1985) Uptake of circulating hyaluronic acid by the rat liver: Cellular localization in situ. *Cell Tissue Res* 242: 505–510.
2. Schledzewski K, et al. (2011) Deficiency of liver sinusoidal scavenger receptors stabilin-1 and -2 in mice causes glomerulofibrotic nephropathy via impaired hepatic clearance of noxious blood factors. *J Clin Invest* 121:703–714.
3. Politz O, et al. (2002) Stabilin-1 and -2 constitute a novel family of fasciclin-like hyaluronan receptor homologues. *Biochem J* 362:155–164.
4. Adachi H, Tsujimoto M (2002) FEEL-1, a novel scavenger receptor with in vitro bacteria-binding and angiogenesis-modulating activities. *J Biol Chem* 277:34264–34270.
5. Hansen B, et al. (2005) Stabilin-1 and stabilin-2 are both directed into the early endocytic pathway in hepatic sinusoidal endothelium via interactions with clathrin/AP-2, independent of ligand binding. *Exp Cell Res* 303:160–173.
6. Kzhyshkowska J, et al. (2005) Phosphatidylinositide 3-kinase activity is required for stabilin-1–mediated endosomal transport of acLDL. *Immunobiology* 210:161–173.
7. Kzhyshkowska J, et al. (2008) Alternatively activated macrophages regulate extracellular levels of the hormone placental lactogen via receptor-mediated uptake and transcytosis. *J Immunol* 180:3028–3037.
8. Kzhyshkowska J, et al. (2006) Novel function of alternatively activated macrophages: Stabilin-1-mediated clearance of SPARC. *J Immunol* 176:5825–5832.
9. Salmi M, Koskinen K, Henttinen T, Elima K, Jalkanen S (2004) CLEVER-1 mediates lymphocyte transmigration through vascular and lymphatic endothelium. *Blood* 104: 3849–3857.
10. Nonaka H, Tanaka M, Suzuki K, Miyajima A (2007) Development of murine hepatic sinusoidal endothelial cells characterized by the expression of hyaluronan receptors. *Dev Dyn* 236:2258–2267.
11. Park SY, et al. (2008) Rapid cell corpse clearance by stabilin-2, a membrane phosphatidylserine receptor. *Cell Death Differ* 15:192–201.
12. Gustafson S, Björkman T (1997) Circulating hyaluronan, chondroitin sulphate and dextran sulphate bind to a liver receptor that does not recognize heparin. *Glycoconj J* 14:561–568.
13. Harris EN, Weigel PH (2008) The ligand-binding profile of HARE: Hyaluronan and chondroitin sulfates A, C, and D bind to overlapping sites distinct from the sites for heparin, acetylated low-density lipoprotein, dermatan sulfate and CS-E. *Glycobiology* 18:638–648.
14. Kogan G, Soltés L, Stern R, Gemeiner P (2007) Hyaluronic acid: A natural biopolymer with a broad range of biomedical and industrial applications. *Biotechnol Lett* 29: 17–25.
15. Fraser JR, Laurent TC, Laurent UB (1997) Hyaluronan: Its nature, distribution, functions and turnover. *J Intern Med* 242:27–33.
16. Stern R, Asari AA, Sugahara KN (2006) Hyaluronan fragments: An information-rich system. *Eur J Cell Biol* 85:699–715.
17. Almond A (2007) Hyaluronan. *Cell Mol Life Sci* 64:1591–1596.
18. Jiang D, et al. (2005) Regulation of lung injury and repair by Toll-like receptors and hyaluronan. *Nat Med* 11:1173–1179.
19. DeGrendele HC, Estess P, Siegelman MH (1997) Requirement for CD44 in activated T cell extravasation into an inflammatory site. *Science* 278:672–675.
20. Zöller M (2011) CD44: Can a cancer-initiating cell profit from an abundantly expressed molecule? *Nat Rev Cancer* 11:254–267.
21. Banerji S, et al. (1999) LYVE-1, a new homologue of the CD44 glycoprotein, is a lymph-specific receptor for hyaluronan. *J Cell Biol* 144:789–801.
22. Kim S, et al. (2009) Carcinoma-produced factors activate myeloid cells through TLR2 to stimulate metastasis. *Nature* 457:102–106.
23. Sironen RK, et al. (2011) Hyaluronan in human malignancies. *Exp Cell Res* 317: 383–391.
24. Toole BP (2004) Hyaluronan: From extracellular glue to pericellular cue. *Nat Rev Cancer* 4:528–539.
25. Twarock S, et al. (2011) Inhibition of oesophageal squamous cell carcinoma progression by in vivo targeting of hyaluronan synthesis. *Mol Cancer* 10:30.
26. Kudo D, et al. (2004) Effect of a hyaluronan synthase suppressor, 4-methylumbelliferone, on B16F-10 melanoma cell adhesion and locomotion. *Biochem Biophys Res Commun* 321:783–787.
27. Zhou B, Weigel JA, Fauss L, Weigel PH (2000) Identification of the hyaluronan receptor for endocytosis (HARE). *J Biol Chem* 275:37733–37741.
28. Harris EN, Weigel JA, Weigel PH (2008) The human hyaluronan receptor for endocytosis (HARE/Stab2) is a systemic clearance receptor for heparin. *J Biol Chem* 283: 21453–21461.
29. Gale NW, et al. (2007) Normal lymphatic development and function in mice deficient for the lymphatic hyaluronan receptor LYVE-1. *Mol Cell Biol* 27:595–604.
30. Yoshihara S, et al. (2005) A hyaluronan synthase suppressor, 4-methylumbelliferone, inhibits liver metastasis of melanoma cells. *FEBS Lett* 579:2722–2726.
31. Takeshita F, et al. (2005) Efficient delivery of small interfering RNA to bone-metastatic tumors by using atelocollagen in vivo. *Proc Natl Acad Sci USA* 102:12177–12182.
32. Jenkins DE, Hornig YS, Oei Y, Dusich J, Purchio T (2005) Bioluminescent human breast cancer cell lines that permit rapid and sensitive in vivo detection of mammary tumors and multiple metastases in immune deficient mice. *Breast Cancer Res* 7:R444–R454.

Advanced Drug Delivery Reviews 65 (2013) 383–390

Contents lists available at SciVerse ScienceDirect

Advanced Drug Delivery Reviews

journal homepage: www.elsevier.com/locate/addr

# Imaging exosome transfer from breast cancer cells to stroma at metastatic sites in orthotopic nude-mouse models☆

Atsushi Suetsugu [a,b,c,1], Kimi Honma [a,b,d,1], Shigetoyo Saji [c], Hisataka Moriwaki [c], Takahiro Ochiya [d], Robert M. Hoffman [a,b,*]

[a] AntiCancer, Inc., San Diego, CA, USA
[b] Department of Surgery, University of California, San Diego, CA, USA
[c] Gifu University Graduate School of Medicine, Gifu, Japan
[d] Division of Molecular and Cellular Medicine, National Cancer Center Research Institute, Tokyo, Japan

ARTICLE INFO

*Article history:*
Accepted 1 August 2012
Available online 17 August 2012

*Keywords:*
Exosome
GFP
RFP
Imaging
Breast cancer
Metastasis
CD63

ABSTRACT

Exosomes play an important role in cell-to-cell communication to promote tumor metastasis. In order to image the fate of cancer-cell-derived exosomes in orthotopic nude mouse models of breast cancer, we used green fluorescent protein (GFP)-tagged CD63, which is a general marker of exosomes. Breast cancer cells transferred their own exosomes to other cancer cells and normal lung tissue cells in culture. In orthotopic nude-mouse models, breast cancer cells secreted exosomes into the tumor microenvironment. Tumor-derived exosomes were incorporated into tumor-associated cells as well as circulating in the blood of mice with breast cancer metastases. These results suggest that tumor-derived exosomes may contribute to forming a niche to promote tumor growth and metastasis. Our results demonstrate the usefulness of GFP imaging to investigate the role of exosomes in cancer metastasis.



**Contents**



## 1. Introduction

Exosomes are small (30–100 nm) membrane vesicles that originate from the endosomal membrane compartment [1]. Recently, it has been demonstrated that cells shed exosomes containing significant amounts of mRNAs, miRNAs and proteins for transferring genetic and proteomic information to target cells as a way of cell-to-cell communication [1–3]. Cancer cells actively release their exosomes into the tumor microenvironment and peripheral blood of cancer patients [1,4].

☆ This review is part of the *Advanced Drug Delivery Reviews* theme issue on "Exosomes: a key to delivering genetic materials".

* Corresponding author at: AntiCancer, Inc., 7917 Ostrow Street, San Diego, CA 92111, USA. Tel.: +1 858 654 2555; fax: +1 858 268 4175.
*E-mail address:* all@anticancer.com (R.M. Hoffman).

[1] These authors contributed equally to this work.

0169-409X/$ – see front matter © 2012 Elsevier B.V. All rights reserved.
http://dx.doi.org/10.1016/j.addr.2012.08.007